

# Computational statistics of segregation and dislocation activities of hydrogen charged free surfaces and grain boundaries

Matthew J. Melfi<sup>1</sup> and S. Mohadeseh Taheri-Mousavi<sup>1,2,\*</sup>

<sup>1</sup>Department of Materials Science and Engineering, Carnegie Mellon University, 5000 Forbes Avenue, Pittsburgh, PA, 15213

<sup>2</sup>Department of Mechanical Engineering, Carnegie Mellon University, 5000 Forbes Avenue, Pittsburgh, PA, 15213

\*Corresponding author: smtaherimousavi@cmu.edu

January 22, 2025

## Abstract

Revealing statistics of H-defect interactions provides insights into significant ductility loss due to the particular strain partitioning in H-charged structural alloys. Experimental investigation of these interactions is extremely difficult, labor-intensive, and costly. Here, we used MD and GCMC simulations and studied H-diffusion deformation at polycrystalline scale with atomic resolution efficiently. To study H-free surface interactions, large pillars including all possible angles and planes of free surfaces were modeled. To study H-grain boundary interactions, several polycrystalline models containing comparable statistics of low and high angle grain boundaries were examined. We studied the statistics of H-segregation tendencies based on free surface angles and grain boundary types. Dislocation activities were also classified for these various types and total density and strength were compared and analyzed compared to H-free samples. In the free surface model, it was observed that H was evenly distributed along the model's surface. Although the dislocation density was reduced compared to H-free samples, localized bands of dislocations were produced. Additionally in the polycrystalline samples, it was concluded that H tends to segregate along grain boundaries with misorientation angles  $\leq 25^\circ$ . However, specific misorientation angle interactions -namely  $>45^\circ$ - led to increased dislocation density in H-charged samples compared to their H-free counterparts.

## 1 Introduction

Hydrogen embrittlement (HE) has been one of the most debated topics in high-strength metallic materials for more than a century<sup>[1, 2]</sup>. HE has led to a reduction in ductility,

fracture resistance, and service life in high-strength metallic alloys. This phenomenon has severely affected several industries with H-rich environments, such as gas and oil, nautical, aerospace, aviation, and automotive fields. Consequently, research efforts to understand HE have substantially increased, with the number of publications on this topic growing exponentially over the past 25 years<sup>[3]</sup>.

These studies proposed multiple theories to explain the HE phenomena. Two main theories, H-enhanced decohesion (HEDE) and H-enhanced localized plasticity (HELP)<sup>[2-52]</sup>, have shown the most amount of discussions. Generally, under deformation, cracks propagate either along grain or phase boundaries or inside grains, depending on which has a lower cohesive energy. In some H-charged samples, however, it was observed that cracks mainly propagate along the boundaries. According to HEDE, this phenomena is the consequence of a lowering of the cohesive energy enough to be lower than the bulk material. As the H concentration increases, the cohesive energy continues to decrease<sup>[49-52]</sup>.

Recently, HELP has sparked significant discussions, yet a centralized definition of this theory and its underlying mechanisms remain elusive. Generally in H-free cracked surfaces, the samples have diffused plasticity around the crack surfaces, and under deformation, the crack tip becomes blunted. Interestingly, when the sample is charged with H, the plasticity distribution has been enhanced and changed to be a narrow band under the crack surfaces. Under deformation of the H-charged samples, this sharp crack remains sharp as it propagates through this narrow plasticity band. There are several proposed explanations aimed at shedding light on this theory. One of these is the concept of lowering the dislocation-dislocation repulsions due to H atmosphere surrounding dislocations. This altered stress field creates a shielding effect around the dislocations, modifying their interaction energy with various obstacles such as secondary phases, solute atoms, and other dislocations. This lowered interaction energy leads to increased dislocation mobility<sup>[28, 42-46]</sup>. This proposed mechanism was debated in a computational study<sup>[20]</sup>. Another proposed explanation involves the lowering of the dislocation formation energy. Consequently, this reduction enhances the nucleation rates of dislocation kink-pairs, regions where the dislocation line deviates from its straight path due to impurities, lattice defects, or other imperfections. If kink-pair formation is considered the rate-limiting step for dislocation motion, higher nucleation rates result in increased dislocation mobility<sup>[40, 41, 53]</sup>. A third explanation involves a reduction in stacking fault energy. A lower stacking fault energy leads to wider stacking faults, which can hinder the cross-slip of dislocations. This restriction forces slip to occur on a single plane, thereby increasing the likelihood of crack propagation<sup>[33-36, 54-56]</sup>.

Numerous studies have utilized various experimental methods to gain insights into HE at different length scales. Tensile tests are commonly employed to compare the performance of H-free and H-charged samples. However, these tests do not provide detailed information about the specific location of H or H-defect interactions within the material<sup>[13, 14, 16, 42]</sup>. Some researchers have utilized electron backscatter diffraction (EBSD) to understand defect interactions such as grain interactions<sup>[57-63]</sup>. Although the source of plasticity, dislocation emissions, and interactions, cannot be tracked explicitly the total effect of dislocation density on deformation gradient can be captured by EBSD. Nevertheless, these efforts have yet to conclusively demonstrate plasticity below the crack surfaces or establish a clear connection between observed deformation mechanisms and microstructural features like grain boundary orientation or dislocation density, primarily due to their large scale. Similarly, the

location of H remains elusive, validating its presence at each defect type cannot be tracked explicitly<sup>[11, 15, 64]</sup>. Cryogenic Atom Probe Tomography (APT), the most advanced experimental method for investigating segregation tendencies, has been employed to study H-defect interactions. With this method, researchers can finally comprehend the precise location of H. However, because these experiments are conducted at cryogenic temperatures, H kinetics are frozen and the room temperature H-defects interactions are not yet thoroughly understood. Moreover, the APT samples are at angstrom scale and thus the high cost of this method does not allow statistical analysis of H-segregation tendencies. Furthermore, this method cannot be applied during deformation of H-charged samples to dynamically track H diffusion at various combinations of defects during deformation<sup>[8, 30]</sup>. As a result, the H-defect interactions at large scale remain elusive in experimental techniques.

Given the uncertainties and challenges inherent in experimental methods in explicitly H tracking, numerical simulations such as molecular dynamics (MD), density functional theory (DFT), and Monte Carlo (MC) simulations have been applied to understand H-defect interactions. MD simulations have been used to study both equilibrium and non-equilibrium processes, while MC simulations are able to capture equilibrium state mechanisms. DFT, by contrast, offers an atomistic perspective on H-defect interactions at the quantum mechanical level<sup>[65–73]</sup>. However, many simulation attempts have length scale limitations and mainly focused solely on a single defect type<sup>[6, 21, 22, 74, 75]</sup> or grain boundary<sup>[4, 6, 7]</sup>. For instance, single-grain investigations typically simulate only a few thousand atoms or a few nanometers in length. Similarly, simulations of grain boundary interactions often examine only a single grain boundary, despite typical samples containing multiple grain boundaries that may interact with one another<sup>[4, 6, 7, 76]</sup>. These simulation types also have their limitations. As mentioned, MD simulations can be performed for equilibrium and non-equilibrium processes but are limited in capturing long time-scale mechanisms such as large-scale diffusion. Conversely, while MC simulations can capture these diffusion mechanisms, they cannot account for non-equilibrium processes such as deformation. Furthermore, they are not efficient in capturing short range equilibrium such as slight relocation of atoms around H atoms when they are inserted during MC steps<sup>[32]</sup>. While offering unparalleled accuracy in calculating the electronic and atomic structures of H-defect interactions, DFT is constrained by high computational costs, limiting its application to small systems of tens to hundreds of atoms.

MC diffusion simulations at the atomistic scale have been conducted using various frameworks, which can be classified into two main categories: those that directly handle the kinetics of diffusion and those that do not. When the actual movements of atoms are not considered, the focus is on the outcome of diffusion, primarily captured by thermodynamics and semiclassical statistical physics. In cases where the kinetics of diffusion is addressed, the kinetic MC technique is the most viable approach.

For simulations that do not handle atomic movements directly, different ensembles are considered based on the type of alloying elements and the target thermodynamic properties. For interstitial alloying elements, such as H, grand canonical Monte Carlo (GCMC) simulations are commonly used<sup>[32, 77, 78]</sup>. These simulations allow for the insertion or deletion of elements at a given chemical potential or partial pressure. It is noteworthy that in all these simulations, the indistinguishability of atoms is accounted for, while other quantum effects are ignored<sup>[32]</sup>.

The combination of MD and MC techniques seems ideal for coupled diffusion-deformation

problem such as the H one. However, in practice, the probabilistic nature of the MC scheme and the evolving number of degrees of freedom complicate the efficient implementation and parallelization of hybrid MC-MD techniques. Recently, there have been multiple attempts at creating efficient parallelized MC simulations. Sadigh et al.<sup>[79]</sup> designed and proposed a novel parallelization scheme capable of performing simultaneous MC moves based on domain decomposition. Yamakov<sup>[80]</sup> implemented parallel MD and semi-grand canonical MC simulations using this algorithm to efficiently model the behavior of substitutional alloys. Moeini-Ardakani et al.<sup>[32]</sup> developed and implemented a new GCMC algorithm that is as scalable as MD while being capable of addressing non-pair and many-body potentials. With this library, simulations can be performed to reveal H-defect interactions that have previously eluded researchers.

By using the Moeini-Ardakani et al.<sup>[32]</sup> library, two different models depicting various defect types will be generated to study H-defect interactions: free surfaces and grain boundaries. Each of these models will be used to reveal H-segregation tendencies and the H influence on underlying deformation mechanisms and mainly dislocation activities.

## 2 Methods

### 2.1 Sample generation

A pillar consisting of a single grain was filled with Nickel (Ni) atoms in a (100) orientation, to replicate a free surface. This shape was deliberately chosen to encompass all possible angles and planes, rather than studying each one individually. Two different samples with the following dimensions were modeled: one sample with a diameter of 6 nm and a length of 30 nm, consisting of approximately 75,000 Ni atoms, while the other sample has a diameter of 20 nm and a length of 30 nm, consisting of approximately 830,000 Ni atoms. To study H grain boundary interactions, five different three-dimensional (3D) polycrystalline samples were created with twenty-seven randomly oriented grains. Each of these grain boundary samples has dimensions of 15 nm  $\times$  15 nm  $\times$  15 nm, with an average grain size of 5 nm, consisting of approximately 310,000 Ni atoms. The main distinction among these grain boundary samples lies in the varying grain orientations and thus grain boundary misorientation angles. By creating a single database across the five different samples, the resulting distribution provides a non-biased dataset of low misorientation angles ( $\leq 15^\circ$ ) and high misorientation angles ( $> 15^\circ$ ). In this dataset, 49.17% of the grain boundaries are represented as low misorientation angles and 50.83% as high misorientation angles. Periodic boundary conditions were applied to all directions for each grain boundary sample.

### 2.2 Numerical Setup

MD and GCMC simulations were performed using the library developed by Moeini-Ardakani et al.<sup>[32]</sup> and LAMMPS code<sup>[81]</sup>. The embedded atom method (EAM) potential<sup>[82]</sup> was adapted for Ni and Ni-H interactions. The Nose-Hoover thermostat was used to maintain an ambient temperature of 300 K during the NPT ensemble. The integration time steps were set to 1 fs for the H-free and 0.5 fs for the H-charged samples. Each sample was

initially relaxed for 500 ps at this temperature under NPT ensemble. GCMC simulations on  $\mu$ VT ensemble was conducted, allowing for H atoms to be inserted and extracted from the samples. The chemical potential of H was set to -2.462 eV<sup>[12]</sup>.

For the deformation process, LAMMPS was utilized. Before deformation, each sample underwent an initial relaxation period of 200 ps within the NPT ensemble. In the free surface samples, a 100% deformation was applied along the Z-axis. In the grain boundary samples, a 10% deformation was applied along the X-axis. All deformations were executed at a constant strain rate of  $10^9 s^{-1}$ .

### 2.3 Post-processing analysis

The H atom coordinates were converted into polar coordinates to evaluate H-segregation tendencies along the free surface samples, particularly across different rotational angles. The Z-coordinate was used to assess H-segregation along the length of the free surface samples. To investigate segregation tendencies along the grain boundaries, the common neighbor analysis modifier (CNA)<sup>[83]</sup> from the Open Visualization Tool (OVITO) was applied, using a cut-off distance of 1 nm<sup>[83, 84]</sup>. This method identifies the atoms surrounding an H atom, enabling the determination of the surrounding grains and, consequently, the identification of the misorientation angle.

To analyze dislocation densities in the free surface samples, the Gaussian density method was employed through the construct surface modifier<sup>[85]</sup>. This was used to determine the pillar volume, while the dislocation analysis (DXA) modifier<sup>[86]</sup> in OVITO was applied to identify and analyze dislocations.

For the grain boundary samples, polyhedral template matching (PTM)<sup>[87]</sup> and grain segmentation<sup>[88]</sup> modifiers were applied to identify grains within the polycrystalline model. DXA was then used to identify and analyze dislocations. The combined use of these modifiers effectively removes dislocations along the grain boundaries, isolating only those emitted within the grains.

In each of these models, the aforementioned modifiers were applied to each frame. However, when using DXA, the dislocation ID values change from frame to frame. To address this issue, a dislocation tracking system was implemented to track the development of dislocations across frames. This was achieved by comparing the dislocation core atoms between consecutive frames throughout the deformation process and calculating a Jaccard similarity score<sup>[89, 90]</sup>, as shown in Eq. (1). In this context,  $A$  and  $B$  represent the lists of dislocation core atoms being compared,  $f$  denotes the frame number,  $i$  and  $j$  refer to the dislocation IDs, and  $m$  and  $n$  indicate the final dislocation IDs in the corresponding frames.

$$J(A_{i,f}, B_{j,f+1}) = \frac{|A_{i,f} \cap B_{j,f+1}|}{|A_{i,f} \cup B_{j,f+1}|}, \quad \begin{cases} i = 0, 1, 2, \dots, m \\ j = 0, 1, 2, \dots, n \end{cases} \quad (1)$$

The maximum Jaccard similarity score was used to track dislocations from frame to frame. However, if no similarity existed between  $A$  and  $B$ , the dislocation was classified as a new dislocation. In such cases, the head and tail -representing the two ends of the dislocation- were analyzed to determine their origins. This process involved selecting the closest dislocation core atom to both the head and tail, then expanding the selection to

include all atoms within a 1 nm cut-off distance to identify the surrounding atoms. In the polycrystalline samples, these selected atoms were then used to identify the grains and misorientation angle. Additionally in the free surface samples, the atoms were converted to polar coordinates to evaluate emission tendencies across different rotational angles. These atoms were also analyzed to assess dislocation emission along the length of the free surface samples using the Z-coordinate.

### 3 Results

#### 3.1 Free Surface

As previously discussed, a pillar made of a single-grain crystal of Ni was used to simulate a free surface. Each sample underwent H-charging, as shown in Figure (1a) and (1b). This reveals that H tends to segregate along the free surface rather than penetrating deeper into the sample. To further explore this H-segregation, each sample was divided into rotational angles in  $30^\circ$  increments and subdivided into 3 nm sections along the Z-axis, Figure (1c). As illustrated in Figure (2), H is uniformly distributed across the rotational angles and along the Z-axis and no particular angles and lengths had noticeable differences compared to others.

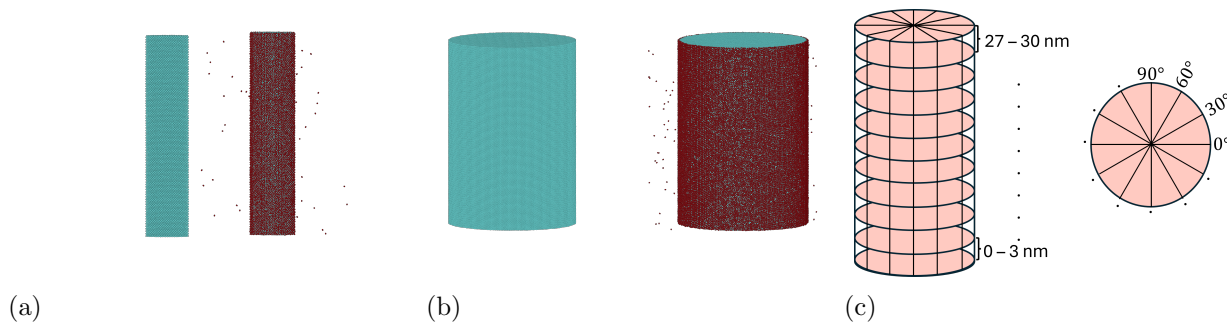


Figure 1: H-free (left) and H-charged (right) samples with a 6 nm diameter and 30 nm length (a) and samples with a 20 nm diameter and 30 nm length (b). (c) Schematic illustrating various length and rotational angles.

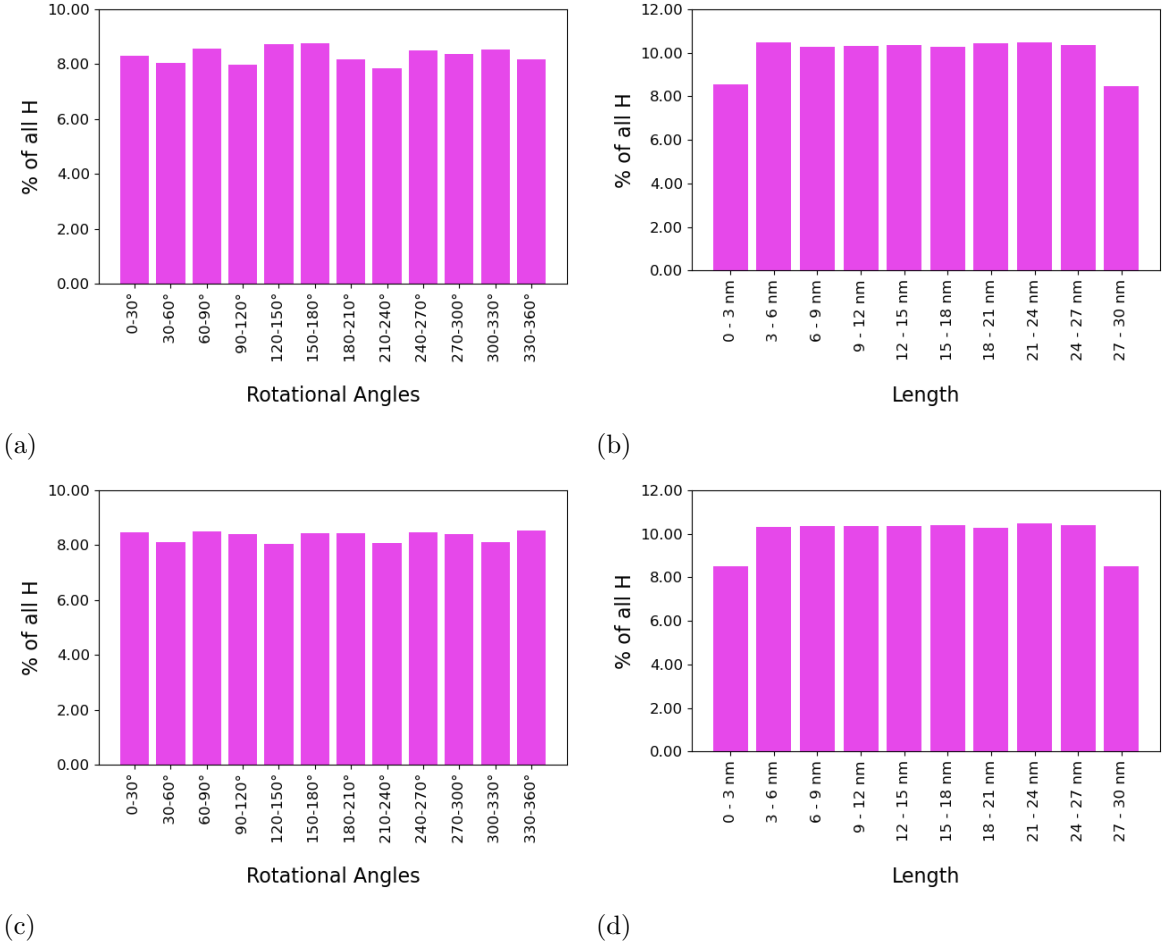
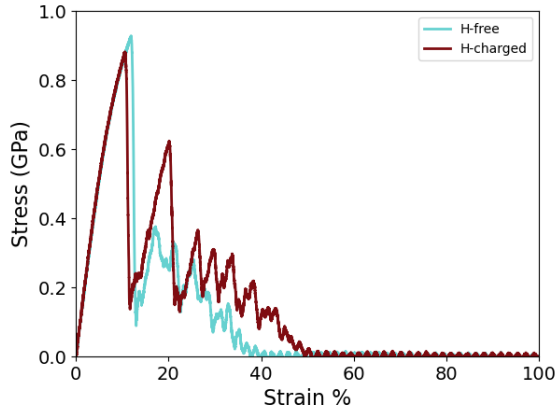
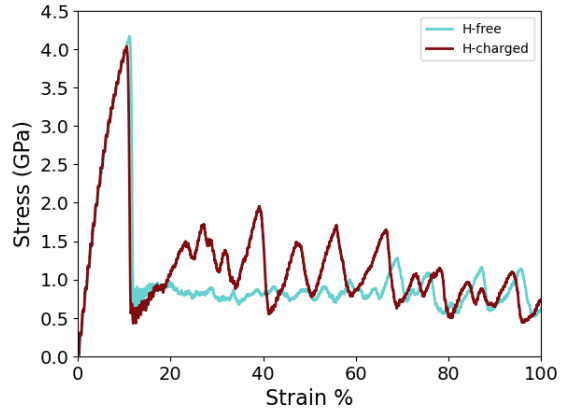


Figure 2: H-segregation along various rotational angles (a) and lengths (b) along the 6 nm diameter and 30 nm length sample and various rotational angles (c) and lengths (d) along the 20 nm diameter and 30 nm length sample.

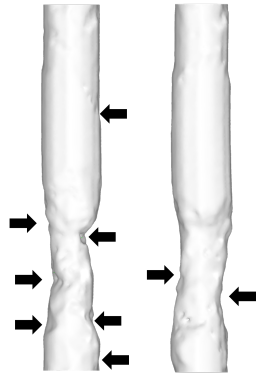
To investigate the mechanical behavior, the samples were deformed along the Z-axis, and the stress-strain responses of H-free and H-charged samples were compared, as shown in Figure (3a) and (3b). In the H-free samples, the stress values obtained were higher than those of the H-charged samples, indicating greater sample strength. While the stress-strain curve of the H-free samples remains relatively flat after the initial deformation for both sample sizes, the H-charged samples display a sawtooth pattern following the initial deformation. This unique behavior can be attributed to differences in dislocation growth and emission across the samples. Further analysis will focus on understanding the role of dislocation activity in these differences.



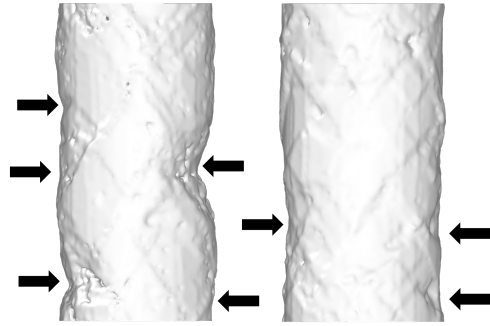
(a)



(b)



(c)



(d)

Figure 3: Stress-strain curves for H-free and H-charged samples with a 6 nm diameter and 30 nm length (a) and a 20 nm diameter and 30 nm length (b). Deformation at 25% strain for H-free (left) and H-charged (right) samples with a 6 nm diameter and 30 nm length (c) and a 20 nm diameter and 30 nm length (d).

As depicted in Figure (4), the H-charged samples exhibit a lower total dislocation density compared to their H-free counterparts. Furthermore, the deformed samples are different in both cases. Figure (3c) and (3d) demonstrates that the H-free samples experience deformation across multiple regions, whereas the H-charged samples show deformation concentrated in a single, localized region. This suggests that H not only influences dislocation density but also affects how deformation is distributed within the material.



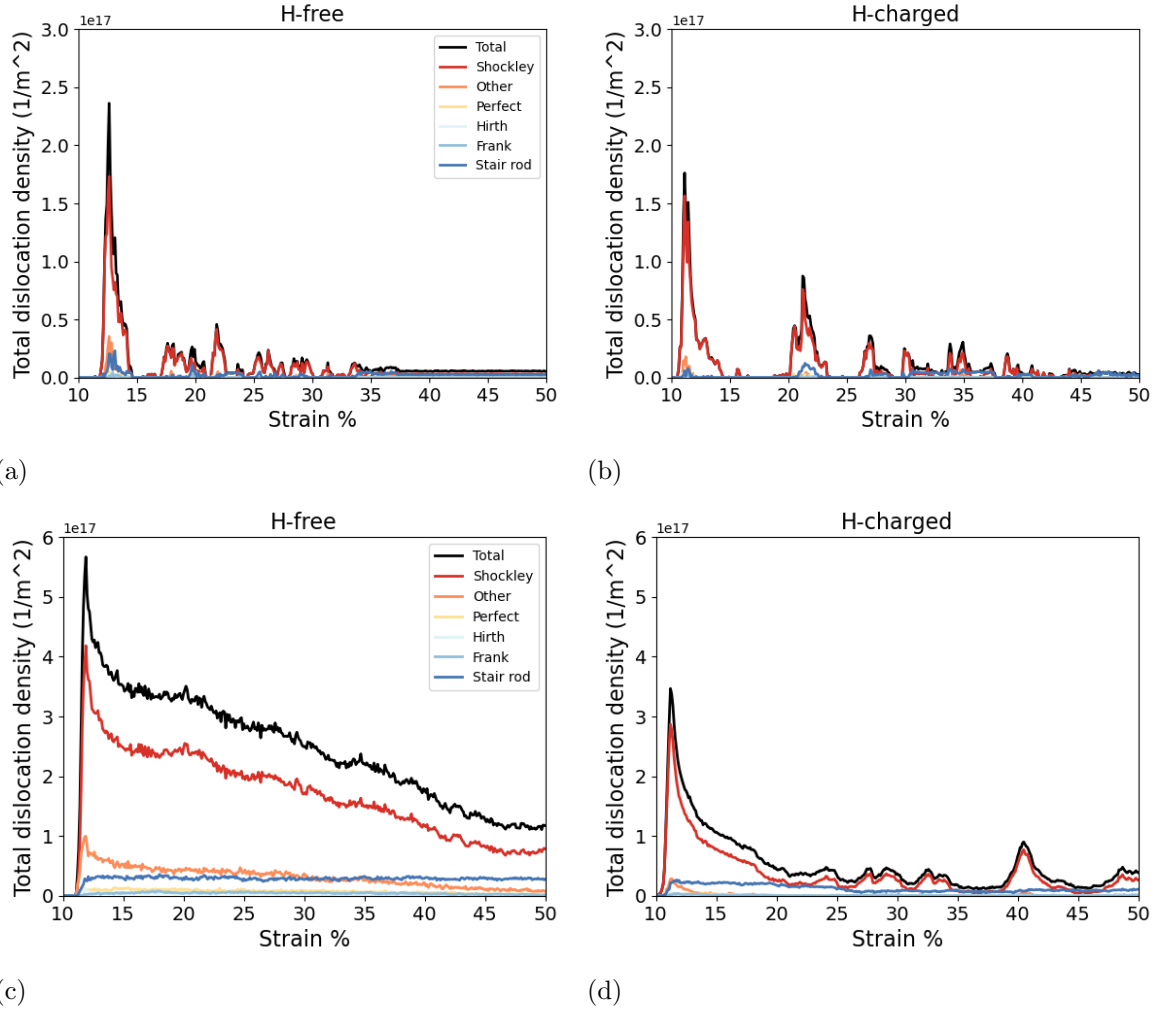


Figure 4: Distribution of dislocation densities for H-free (a) and (c) and H-charged (b) and (d) samples with a 6 nm diameter and 30 nm length and a 20 nm diameter and 30 nm length respectively.

Dislocations were tracked throughout the deformation process to identify where the head and tail were emitted from the initially undeformed samples. This analysis was conducted in the same subsections as previously defined in Figure (1c). To assess the effect of H on dislocation density in each subsection, the H-charged values were normalized against the H-free values. However, if the dislocation density in the H-free samples was zero, the H-charged dislocation density is presented directly. Figure (5) shows the values for both the angle and Z-axis. While no clear trend is observed for the rotational angle, the Z-axis plot reveals an increased concentration of dislocation emission in the 6-9 nm regions of the H-charged samples compared to the H-free samples. This region aligns with the localized deformed region shown in Figure (3c) and (3d). The presence of this localized region in the H-charged sample also brings support for the HELP theory.

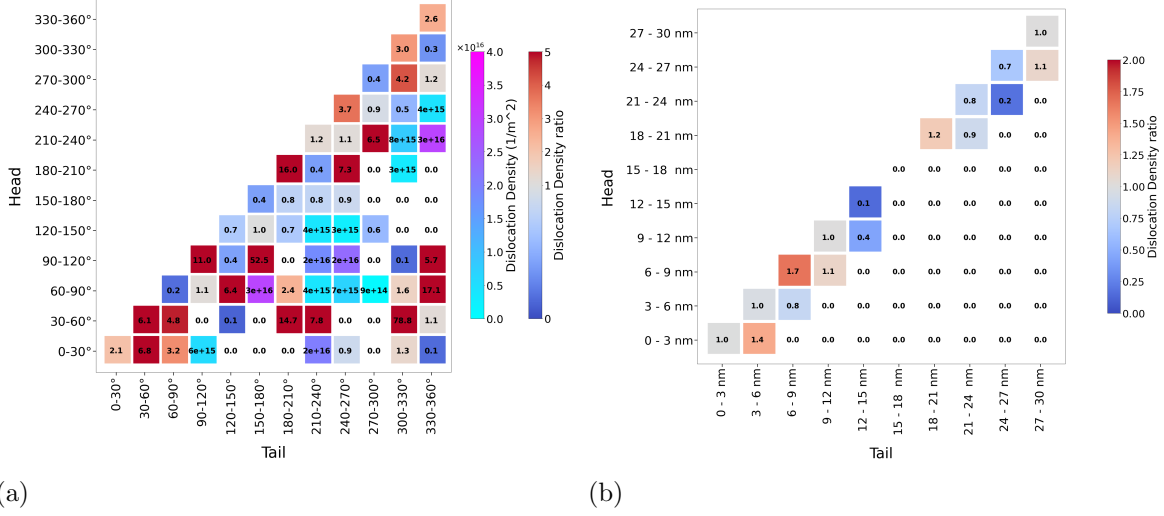


Figure 5: Normalized dislocation densities as a function of various rotational angles (a) and length regions (b), for the 6 nm diameter and 30 nm length free surface sample.

### 3.2 Grain Boundary

As mentioned, five different samples, each containing twenty-seven grains, underwent H charging. In these grain boundary samples, H tends to segregate along the grain boundaries. Specifically, 52.72% of all H segregates along low misorientation angles. A closer examination of the H-segregation pattern, shown in Figure (6b), reveals three key regions: the first corresponds to misorientation angles  $\leq 25^\circ$ ; the second, misorientation angles 25-45°; and the third, misorientation angles  $> 45^\circ$ . Although the transition from low to high misorientation angles occurs at 15°, providing a well-balanced dataset, a clear preference for H-segregation is observed. Specifically, 77.50% of all H segregates at misorientation angles  $\leq 25^\circ$ .

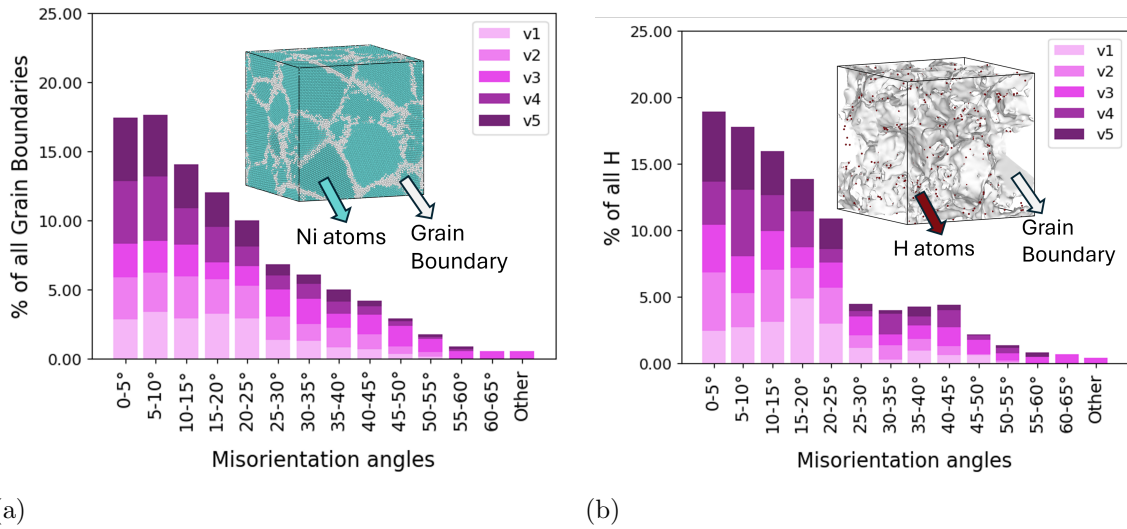
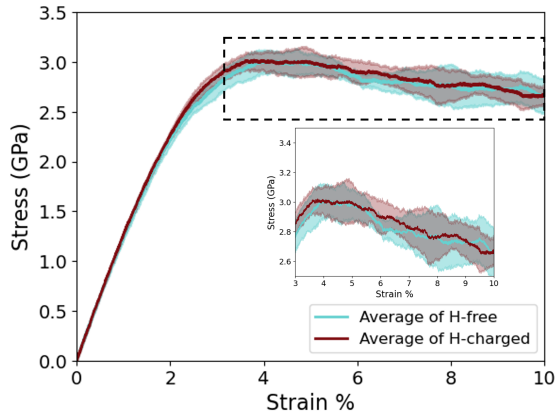
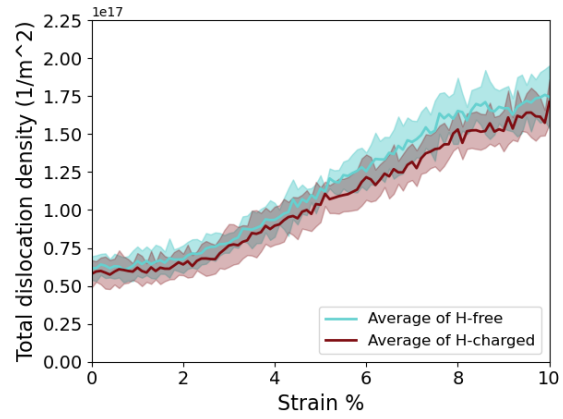


Figure 6: (a) Distribution of all Grain boundaries according to their misorientation angle. (b) H-segregation tendencies according to grain boundary misorientation angle.

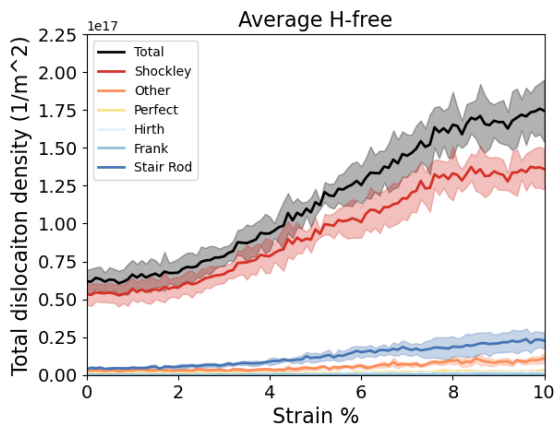
To analyze the mechanical behavior, the samples were deformed along the X-axis, and the average responses of the H-free and H-charged samples were compared. Globally, there is minimal change between the H-free and H-charged curves. However, closer inspection of the plastic region reveals that the inclusion of H results in higher stress within the samples. In these samples, the increased stress in H-charged samples can be attributed to a decrease in dislocation density within the grains.



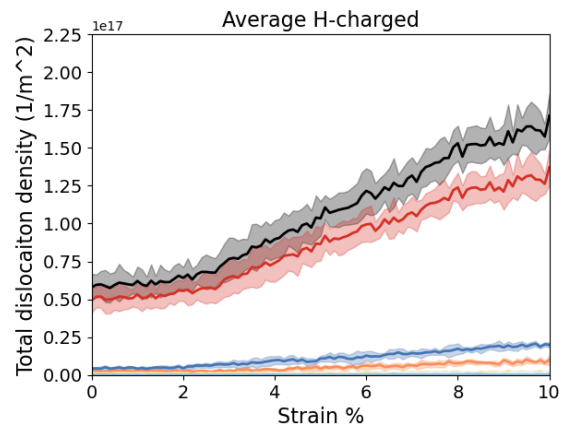
(a)



(b)



(c)



(d)

Figure 7: (a) Average stress-strain curves for each of the grain boundary samples. (b) Average total dislocation density for H-free and H-charged grain boundary samples. Average distribution of dislocation densities for H-free (c) and H-charged (d) grain boundary samples.

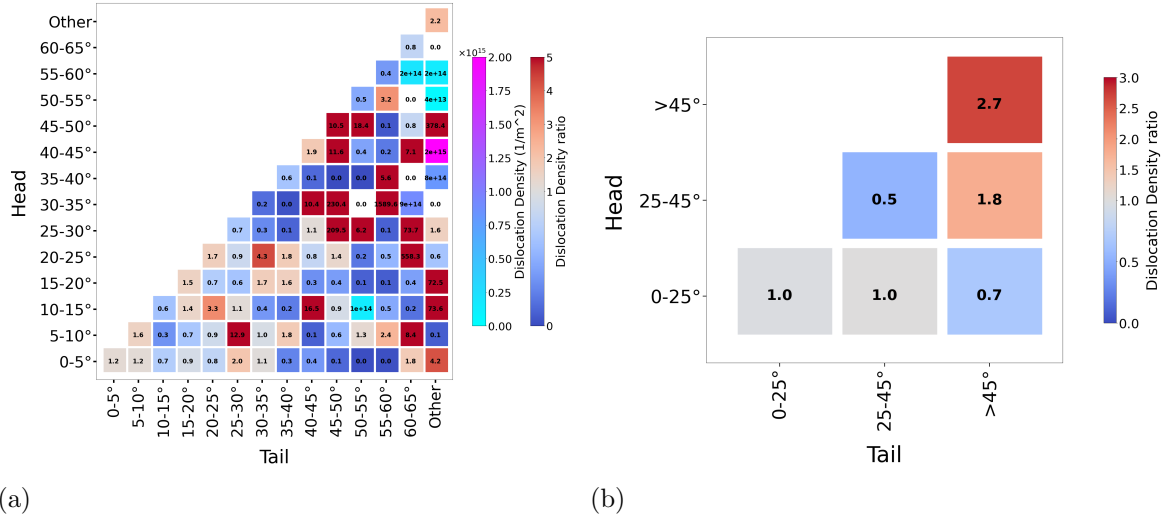


Figure 8: (a) Normalized dislocation densities as a function of various misorientation angles (b) Simplified version of (a) according to H-segregation regions.

Similar to how the dislocations were tracked in the free surface samples, the dislocations were tracked to determine which misorientation angle the head and tail were emitted from. Once more, the H-charged values were normalized against the H-free values to assess the effect of H on the average dislocation density. Figure (8) shows these values concerning the misorientation angle. In the misorientation angles  $\leq 25^\circ$ , there is minimal dislocation density change. However, when looking at the misorientation angles  $\geq 25^\circ$  there is a clear increase change in dislocation density. By taking the key regions of H-segregation into account Figure (8a) can be simplified into Figure (8b), by combining the various regions.

This variation in dislocation density may be due to H altering the activation energy of dislocations. Specifically, H could either increase the activation energy for low misorientation angles to a point where the activation energy for high misorientation angles becomes lower, or it could reduce the activation energy of high misorientation angles to where it is lower than that of low misorientation angles.

## 4 Discussion

In these models, H atoms tend to concentrate in regions where their incorporation into the microstructure requires less energy. In the free surface models, H favors segregation along the surface rather than within the bulk material. At the free surface, atoms are less coordinated with their neighbors compared to the bulk, where atoms are part of a more stable, uniform structure with no gaps in atomic sites. This difference creates a region along the free surface that requires less energy for H to be inserted. Additionally, introducing H increases the local coordination number, which raises the energy required to insert additional H atoms at the same site.

For typical interstitial alloys, atoms are often seen to segregate along high-angle grain boundaries rather than low-angle grain boundaries<sup>[91-101]</sup>. High-angle grain boundaries exhibit greater atomic misorientation and disordered regions<sup>[99-101]</sup>, which create larger in-

terstitial sites and enhanced diffusion paths<sup>[100–104]</sup>. These characteristics make it easier for interstitial atoms, like Carbon and Nitrogen<sup>[91–94]</sup>, to segregate along high-angle grain boundaries. In contrast, low-angle grain boundaries have a more ordered structure, offering fewer and smaller interstitial sites compared to high-angle grain boundaries.

However, we hypothesize that H behaves differently from typical interstitial atoms along grain boundaries due to its small atomic size and high diffusivity. Low-angle grain boundaries are composed of ordered structures and stable sites where tiny H can settle at lower energy than in the unstable sites available in disordered regions of high-angle grain boundaries. The sites on high-angle grain boundaries can be more unstable for H, as it can continuously diffuse and relocate to other available sites.

Experimental validation efforts in the literature have utilized silver-decoration EBSD to investigate H permeation tendencies. In this method, a solution containing silver ions is applied to the surface of the sample. These silver ions are reduced by the H atoms diffusing into the sample, resulting in the formation of silver nanoparticles<sup>[105, 106]</sup>. The presence of these silver nanoparticles act as an indirect way of mapping H diffusion pathways into the material. Some studies have shown a greater accumulation of silver nanoparticles along high-angle misorientation grain boundaries compared to low-angle misorientation grain boundaries<sup>[60, 62, 63]</sup>. In addition, simulations in the literature have explored H diffusion along grain boundaries. These simulations suggest that low-angle grain boundaries impede H diffusion, while high-angle grain boundaries either maintain or accelerate the diffusion<sup>[107–112]</sup>.

The silver-decoration studies imply that H enters the sample through high-angle grain boundaries, diffusing along these boundaries<sup>[60, 62, 63, 105, 106]</sup>. However, this experiment does not necessary prove where H finally segregate. When H encounters low-angle grain boundaries, the diffusion of H slows, as corroborated by H diffusion simulations<sup>[107–112]</sup>, and in eventually segregate along these boundaries. Our results thus are not in contradict with these silver decoration experiments as they mainly locate H diffusion paths, and not necessary segregation sites.

Additionally, experimental approaches, such as cryogenic APT, have been used to measure the distribution of H at dislocations, grain boundaries, and precipitates<sup>[113–115]</sup>. This method has successfully identified the presence of H at these defects. However, many of these studies focus on a single high misorientation grain boundary, which may not fully capture the complete H-segregation tendencies when various types of grain boundaries are available<sup>[116, 117]</sup>.

Considering dislocation emission, growth, and deformation, the free surface samples analyzed in this study reveal a distinct difference between H-free and H-charged samples. As previously discussed, the H-free samples exhibit multiple regions of deformation, whereas the H-charged samples display a single, localized deformation region. This deformation pattern aligns with experimental observations in H-free and H-charged pentatwinned samples reported by Yin et al.<sup>[118]</sup>. In the same study, the presence of H was shown to hinder dislocation nucleation, thereby increasing the energy required for dislocation emission as was calculated by Nudged Elastic Band (NEB) simulations<sup>[118]</sup>.

Experimental studies in the literature have employed various techniques, such as environmental transmission electron microscopy (ETEM) and scanning electron microscopy-based electron channeling contrast imaging (SEM-based ECCI), to investigate dislocation activity near grain boundaries under deformation. Both methods, ETEM and SEM-based ECCI,

have demonstrated, in the absence of H, dislocations exhibit a certain level of mobility and density<sup>[12, 45, 60, 119–125]</sup>. However, with the presence of H, these dislocations displayed increased mobility, suggesting that H plays a promoting role in dislocation mobility and nucleation.

Contrasting to experimental attempts, simulation studies have reported conflicting results regarding dislocation density in the presence of H. Some of the studies indicate a reduction in dislocation density, while others have reported an increase with the presence of H. Some of these discrepancies can be attributed to various factors, including material type, alloying composition, microstructure, H concentration, H diffusivity, applied loading conditions, temperature, stress state, and defect types<sup>[12, 126–129]</sup>. These contradictions underscore the importance of studying the statistics of H-segregation on fair amount of defects, rather than focusing on a limited window in the microstructure. It is also noteworthy that while the MD simulation results depend on the validity of the potential used, the potential employed in this study has been validated multiple times in previous research<sup>[5, 12, 76, 130–137]</sup>. The obtained results here need to be further validated by DFT calculations. This will be reported in our future studies while we appreciate DFT’s limitations in simulating only small and simple case studies of all these defect types.

## 5 Conclusions

Considering all the results presented in this study and relating them to the HELP mechanism, our simulations offer new insights. In the free surface model, H-free samples exhibit multiple regions of deformation due to higher dislocation emissions. This behavior aligns with observations in H-free samples, where crack blunting occurs as a result of dislocation activity at the crack surfaces, which serve as free surfaces. In contrast, H-charged samples displayed concentrated deformation localized in a single region, forming a singular path for crack propagation. This behavior is consistent with H-charged samples, where the sharpness of the crack surfaces is preserved.

In the grain boundary samples analyzed in this study, observations indicate a reduction in dislocation density. This finding does not support with the notion of increased plasticity in tiny ribbons beneath the crack surface as proposed by the HELP theory. Our simulations show that potentially grain boundaries alone cannot explain the increased plastic deformation. This suggests that the combination of defects, e.g., grain boundaries with free surfaces or vacancies, might be responsible for the enhancement. Our grain boundary study support the decreased plasticity far from crack surfaces in H-charged samples. In conclusion, our studies suggest statistical analyses of H on a more comprehensive defect network to unravel the full picture of the HELP mechanism.

## References

- [1] Johnson William. Ii. on some remarkable changes produced in iron and steel by the action of hydrogen and acids. *Proceedings of the Royal Society of London*, 23:168–179, 12 1875.
- [2] Yuh Fukai. Metal-hydrogen system under extended p, t conditions. *Springer*, pages 71–119, 1993.
- [3] Chilou Zhou, Yingjie Ren, Xinrui Yan, Yiran Zheng, and Baoqing Liu. A bibliometric and visualized overview of hydrogen embrittlement from 1997 to 2022. *Energies*, 15, 12 2022.
- [4] Han Lin Mai, Xiang Yuan Cui, Daniel Scheiber, Lorenz Romaner, and Simon P. Ringer. An understanding of hydrogen embrittlement in nickel grain boundaries from first principles. *Materials & Design*, 212:110283, 12 2021.
- [5] Jun Song and W. A. Curtin. Atomic mechanism and prediction of hydrogen embrittlement in iron. *Nature Materials*, 12:145–151, 2 2013.
- [6] Linshuo Dong, Shuize Wang, Guilin Wu, Junheng Gao, Xiaoye Zhou, Hong Hui Wu, and Xinping Mao. Application of atomic simulation for studying hydrogen embrittlement phenomena and mechanism in iron-based alloys. *International Journal of Hydrogen Energy*, 47:20288–20309, 5 2022.
- [7] Sojeong Yang, Sei Hun Yun, and Takuji Oda. Molecular dynamics simulation on stability and diffusivity of hydrogen around a  $\{111\}$  symmetric tilt grain boundary in bcc-fe. *Fusion Engineering and Design*, 131:105–110, 6 2018.
- [8] Huan Zhao, Poulami Chakraborty, Dirk Ponge, Tilmann Hickel, Binhan Sun, Chun Hung Wu, Baptiste Gault, and Dierk Raabe. Hydrogen trapping and embrittlement in high-strength al alloys. *Nature 2022 602:7897*, 602:437–441, 2 2022.
- [9] Binhan Sun, Wenjun Lu, Baptiste Gault, Ran Ding, Surendra Kumar Makineni, Di Wan, Chun Hung Wu, Hao Chen, Dirk Ponge, and Dierk Raabe. Chemical heterogeneity enhances hydrogen resistance in high-strength steels. *Nature Materials 2021 20:12*, 20:1629–1634, 7 2021.
- [10] Muhammad Wasim, Milos B. Djukic, and Tuan Duc Ngo. Influence of hydrogen-enhanced plasticity and decohesion mechanisms of hydrogen embrittlement on the fracture resistance of steel. *Engineering Failure Analysis*, 123, 5 2021.
- [11] Hong Luo, Seok Su Sohn, Wenjun Lu, Linlin Li, Xiaogang Li, Chandrahasan K. Soundararajan, Waldemar Krieger, Zhiming Li, and Dierk Raabe. A strong and ductile medium-entropy alloy resists hydrogen embrittlement and corrosion. *Nature Communications 2020 11:1*, 11:1–8, 6 2020.



- [12] Motomichi Koyama, Mohadeseh Taheri-Mousavi, Haoxue Yan, Jinwoo Kim, Benjamin Clive Cameron, Sina Moeini-Ardakani, Ju Li, and Cemal Cem Tasan. Origin of micrometer-scale dislocation motion during hydrogen desorption. *Sci. Adv*, 6, 2020.
- [13] Di Wan, Antonio Alvaro, Vigdis Olden, and Afrooz Barnoush. Hydrogen-enhanced fatigue crack growth behaviors in a ferritic fe-3wt%si steel studied by fractography and dislocation structure analysis. *International Journal of Hydrogen Energy*, 44:5030–5042, 2 2019.
- [14] Antonio Alvaro, Di Wan, Vigdis Olden, and Afrooz Barnoush. Hydrogen enhanced fatigue crack growth rates in a ferritic fe-3wt%si alloy and a x70 pipeline steel. *Engineering Fracture Mechanics*, 219:106641, 10 2019.
- [15] Hong Luo, Zhiming Li, Wenjun Lu, Dirk Ponge, and Dierk Raabe. Hydrogen embrittlement of an interstitial equimolar high-entropy alloy. *Corrosion Science*, 136:403–408, 5 2018.
- [16] Yun Deng and Afrooz Barnoush. Hydrogen embrittlement revealed via novel in situ fracture experiments using notched micro-cantilever specimens. *Acta Materialia*, 142:236–247, 1 2018.
- [17] Kelly E. Nygren, Shuai Wang, Kaila M. Bertsch, Hongbin Bei, Akihide Nagao, and Ian M. Robertson. Hydrogen embrittlement of the equi-molar fencocr alloy. *Acta Materialia*, 157:218–227, 9 2018.
- [18] Degang Xie, Suzhi Li, Meng Li, Zhangjie Wang, Peter Gumbsch, Jun Sun, Evan Ma, Ju Li, and Zhiwei Shan. Hydrogenated vacancies lock dislocations in aluminium. *Nature Communications*, 7, 2016.
- [19] Ian M. Robertson, P. Sofronis, A. Nagao, M. L. Martin, S. Wang, D. W. Gross, and K. E. Nygren. Hydrogen embrittlement understood. *Metallurgical and Materials Transactions B: Process Metallurgy and Materials Processing Science*, 46:1085–1103, 6 2015.
- [20] J. Song and W. A. Curtin. Mechanisms of hydrogen-enhanced localized plasticity: An atomistic study using  $\alpha$ -fe as a model system. *Acta Materialia*, 68:61–69, 4 2014.
- [21] Ryosuke Matsumoto, Shinya Taketomi, Sohei Matsumoto, and Noriyuki Miyazaki. Atomistic simulations of hydrogen embrittlement. *International Journal of Hydrogen Energy*, 34:9576–9584, 12 2009.
- [22] Mao Wen, Xue Jun Xu, Yuki Omura, Seiji Fukuyama, and Kiyoshi Yokogawa. Modeling of hydrogen embrittlement in single crystal ni. *Computational Materials Science*, 30:202–211, 8 2004.
- [23] H. K. Birnbaum. Hydrogen effects on deformation and fracture: Science and sociology. *MRS Bulletin*, 28:479–485, 1 2003.

- [24] Gang Lu, Qing Zhang, Nicholas Kioussis, and Efthimios Kaxiras. Hydrogen-enhanced local plasticity in aluminum: An ab initio study. *Physical Review Letters*, 87:955011–955014, 8 2001.
- [25] Y. Katz, N. Tymiak, and W. W. Gerberich. Nanomechanical probes as new approaches to hydrogen/deformation interaction studies. *Engineering Fracture Mechanics*, 68:619–646, 4 2001.
- [26] D. Delafosse and T. Magnin. Hydrogen induced plasticity in stress corrosion cracking of engineering systems. *Engineering Fracture Mechanics*, 68:693–729, 4 2001.
- [27] J Lufrano, F P Sofronist, and H K Birnbaum. Modeling of hydrogen transport and elastically accommodated hydride formation near a crack tip. *J. Mech. Phys. Solids*, 44:179–205, 1996.
- [28] H K Birnbaum and P Sofronis. Hydrogen-enhanced localized plasticity—a mechanism for hydrogen-related fracture. *Materials Science and Engineering*, 176:191–202, 1994.
- [29] D. S. Shih, I. M. Robertson, and H. K. Birnbaum. Hydrogen embrittlement of  $\alpha$  titanium: In situ tem studies. *Acta Metallurgica*, 36:111–124, 1 1988.
- [30] Yi-Sheng Chen, Hongzhou Lu, Jiangtao Liang, Alexander Rosenthal, Hongwei Liu, Glenn Sneddon, Ingrid Mccarroll, Zhengzhi Zhao, Wei Li, Aimin Guo, and Julie M Cairney. Observation of hydrogen trapping at dislocations, grain boundaries, and precipitates. *Science*, 2020.
- [31] Fukai Y. The metal-hydrogen system: Basic bulk properties. *Springer*, 2005.
- [32] Seyed Sina Moeini-Ardakani, Seyedeh Mohadeseh Taheri-Mousavi, and Ju Li. Highly efficient parallel grand canonical simulations of interstitial-driven deformation-diffusion processes. *Modelling and Simulation in Materials Science and Engineering*, 29, 2 2021.
- [33] Weijie Wu, Shenguang Liu, Xuewei Zhang, Weiguo Li, and Jinxu Li. Effect of test temperature on the hydrogen embrittlement susceptibility of a duplex stainless steel. *International Journal of Hydrogen Energy*, 7 2023.
- [34] Shinya Taketomi, Ryosuke Matsumoto, and Noriyuki Miyazaki. Atomistic study of the effect of hydrogen on dislocation emission from a mode ii crack tip in alpha iron. *International Journal of Mechanical Sciences*, 52:334–338, 2 2010.
- [35] Y. K. Lee, S. J. Lee, and J. Han. Critical assessment 19: stacking fault energies of austenitic steels. <http://dx.doi.org/10.1080/02670836.2015.1114252>, 32:1–8, 2016.
- [36] Han Jin Kim, Min Kyung Cho, Gyeungho Kim, Seung Yong Lee, Min Gu Jo, Hayoung Kim, Jin Yoo Suh, and Joonho Lee. Influence of hydrogen absorption on stacking fault of energy of a face-centered cubic high entropy alloy. *Metals and Materials International*, 28:2637–2645, 11 2022.

- [37] A. Moreno-Gobbi, G. Zamir, and J. A. Eiras. Ultrasonic investigation of the interaction of hydrogen-dislocations in copper crystals. *Materials Science and Engineering: A*, 528:4255–4258, 5 2011.
- [38] M. Wen, L. Zhang, B. An, S. Fukuyama, and K. Yokogawa. Hydrogen-enhanced dislocation activity and vacancy formation during nanoindentation of nickel. *Physical Review B - Condensed Matter and Materials Physics*, 80:094113, 9 2009.
- [39] H. Matsui, H. Kimura, and S. Moriya. The effect of hydrogen on the mechanical properties of high purity iron i. softening and hardening of high purity iron by hydrogen charging during tensile deformation. *Materials Science and Engineering*, 40:207–216, 10 1979.
- [40] Reiner Kirchheim. Revisiting hydrogen embrittlement models and hydrogen-induced homogeneous nucleation of dislocations. *Scripta Materialia*, 62:67–70, 1 2010.
- [41] Y. Z. Chen, H. P. Barth, M. Deutges, C. Borchers, F. Liu, and R. Kirchheim. Increase in dislocation density in cold-deformed pd using h as a temporary alloying addition. *Scripta Materialia*, 68:743–746, 5 2013.
- [42] Afrooz Barnoush and Horst Vehoff. Recent developments in the study of hydrogen embrittlement: Hydrogen effect on dislocation nucleation. *Acta Materialia*, 58:5274–5285, 9 2010.
- [43] I. M. Robertson. The effect of hydrogen on dislocation dynamics. *Engineering Fracture Mechanics*, 68:671–692, 4 2001.
- [44] May L. Martin, Mohsen Dadfarnia, Akihide Nagao, Shuai Wang, and Petros Sofronis. Enumeration of the hydrogen-enhanced localized plasticity mechanism for hydrogen embrittlement in structural materials. *Acta Materialia*, 165:734–750, 2 2019.
- [45] G. M. Bond, I. M. Robertson, and H. K. Birnbaum. The influence of hydrogen on deformation and fracture processes in high-strength aluminum alloys. *Acta Metallurgica*, 35:2289–2296, 9 1987.
- [46] P. Sofronis. The influence of mobility of dissolved hydrogen on the elastic response of a metal. *Journal of the Mechanics and Physics of Solids*, 43:1385–1407, 9 1995.
- [47] Ju Yao, Qiyang Tan, Jeffrey Venezuela, Andrej Atrens, and Ming Xing Zhang. Recent research progress in hydrogen embrittlement of additively manufactured metals – a review. *Current Opinion in Solid State and Materials Science*, 27, 10 2023.
- [48] Bessemer Pfeil. The effect of occluded hydrogen on the tensile strength of iron. *Proceedings of the Royal Society of London*, 1926.
- [49] M. L. Martin, B. P. Somerday, R. O. Ritchie, P. Sofronis, and I. M. Robertson. Hydrogen-induced intergranular failure in nickel revisited. *Acta Materialia*, 60:2739–2745, 4 2012.

- [50] Alexander R. Troiano. The role of hydrogen and other interstitials in the mechanical behavior of metals: (1959 edward de mille campbell memorial lecture). *Metallography, Microstructure, and Analysis*, 5:557–569, 12 2016.
- [51] Yunlong Li and Keshi Zhang. Analysis of hydrogen-assisted brittle fracture using phase-field damage modelling considering hydrogen enhanced decohesion mechanism. *Metals 2022, Vol. 12, Page 1032*, 12:1032, 6 2022.
- [52] Milos B. Djukic, Gordana M. Bakic, Vera Sijacki Zeravcic, Aleksandar Sedmak, and Bratislav Rajicic. The synergistic action and interplay of hydrogen embrittlement mechanisms in steels and iron: Localized plasticity and decohesion. *Engineering Fracture Mechanics*, 216:106528, 7 2019.
- [53] Reiner Kirchheim. Reducing grain boundary, dislocation line and vacancy formation energies by solute segregation. i. theoretical background. *Acta Materialia*, 55:5129–5138, 9 2007.
- [54] D M Symons. Hydrogen embrittlement of ni-cr-fe alloys. *Springer Nature*, 28, 1997.
- [55] X. W. Zhou, C. Nowak, R. S. Skelton, M. E. Foster, J. A. Ronevich, C. San Marchi, and R. B. Sills. An fe–ni–cr–h interatomic potential and predictions of hydrogen-affected stacking fault energies in austenitic stainless steels. *International Journal of Hydrogen Energy*, 47:651–665, 1 2022.
- [56] Zhouqi Zheng, Shuang Liang, Yaxin Zhu, Minsheng Huang, and Zhenhuan Li. Studying hydrogen effect on the core structure and mobility of dislocation in nickel by atomistically-informed generalized peierls–nabarro model. *Mechanics of Materials*, 140, 1 2020.
- [57] Hide aki NISHIKAWA, Yasuji ODA, Yoshimasa TAKAHASHI, and Hiroshi NOGUCHI. Microscopic observation of the brittle-striation formation mechanism in low carbon steel fatigued in hydrogen gas (tem and ebsd observation corresponding to fractography). *Journal of Solid Mechanics and Materials Engineering*, 5:179–190, 2011.
- [58] A. Laureys, T. Depover, R. Petrov, and K. Verbeken. Microstructural characterization of hydrogen induced cracking in trip-assisted steel by ebsd. *Materials Characterization*, 112:169–179, 2 2016.
- [59] A. Laureys, M. Pinson, T. Depover, R. Petrov, and K. Verbeken. Ebsd characterization of hydrogen induced blisters and internal cracks in trip-assisted steel. *Materials Characterization*, 159, 1 2020.
- [60] Masoud Moshtaghi, Mahdiah Safyari, and Gregor Mori. Combined thermal desorption spectroscopy, hydrogen visualization, hrtem and ebsd investigation of a ni–fe–cr alloy: The role of hydrogen trapping behavior in hydrogen-assisted fracture. *Materials Science and Engineering: A*, 848, 7 2022.

- [61] Claude Fressengeas, Benoît Beausir, Christophe Kerisit, Anne Laure Helbert, Thierry Baudin, François Brisset, Marie H el ene Mathon, R emy Besnard, and Nathalie Bozzolo. On the evaluation of dislocation densities in pure tantalum from ebsd orientation data. *Materiaux et Techniques*, 106, 2018.
- [62] Motomichi Koyama, Daisuke Yamasaki, Tatsuya Nagashima, Cemal Cem Tasan, and Kaneaki Tsuzaki. In situ observations of silver-decoration evolution under hydrogen permeation: Effects of grain boundary misorientation on hydrogen flux in pure iron. *Scripta Materialia*, 129:48–51, 3 2017.
- [63] Jinwoo Kim and Cemal Cem Tasan. Microstructural and micro-mechanical characterization during hydrogen charging: An in situ scanning electron microscopy study. *International Journal of Hydrogen Energy*, 44:6333–6343, 3 2019.
- [64] Hong Luo, Zhiming Li, Wenjun Lu, Dirk Ponge, and Dierk Raabe. Hydrogen embrittlement of an interstitial equimolar high-entropy alloy. *Corrosion Science*, 136:403–408, 5 2018.
- [65] Hye Jin Kim, Soon Hyeok Jeon, Won Seog Yang, Byung Gil Yoo, Yoo Dong Chung, Heon Young Ha, and Hyun Young Chung. Effects of titanium content on hydrogen embrittlement susceptibility of hot-stamped boron steels. *Journal of Alloys and Compounds*, 735:2067–2080, 2 2018.
- [66] Xu Lu, Yan Ma, Yuan Ma, Dong Wang, Lei Gao, Wenwen Song, Lijie Qiao, and Roy Johnsen. Unravelling the effect of f phase on hydrogen-assisted intergranular cracking in nickel-based alloy 725: Experimental and dft study. *Corrosion Science*, 225, 12 2023.
- [67] Tarlan Hajilou, Iman Taji, Frederic Christien, Shuang He, Daniel Scheiber, Werner Ecker, Reinhard Pippan, Vsevolod I. Razumovskiy, and Afrooz Barnoush. Hydrogen-enhanced intergranular failure of sulfur-doped nickel grain boundary: In situ electrochemical micro-cantilever bending vs. dft. *Materials Science and Engineering: A*, 794, 9 2020.
- [68] Gabriel R. Schleder, Antonio C.M. Padilha, Carlos Mera Acosta, Marcio Costa, and Adalberto Fazzio. From dft to machine learning: Recent approaches to materials science - a review. *JPhys Materials*, 2, 7 2019.
- [69] Lixia Zhu, Jinheng Luo, Shunli Zheng, Shuaijun Yang, Jun Hu, and Zhong Chen. Understanding hydrogen diffusion mechanisms in doped alpha-fe through dft calculations. *International Journal of Hydrogen Energy*, 48:17703–17710, 5 2023.
- [70] K. Christmann, R. J. Behm, G. Ertl, M. A. Van Hove, and W. H. Weinberg. Chemisorption geometry of hydrogen on ni(111): Order and disorder. *The Journal of Chemical Physics*, 70:4168–4184, 1979.
- [71] K. Christmann, O. Schober, G. Ertl, and M. Neumann. Adsorption of hydrogen on nickel single crystal surfaces. *The Journal of Chemical Physics*, pages 4528–4540, 1974.

- [72] Peter Ferrin, Shampa Kandoi, Anand Udaykumar Nilekar, and Manos Mavrikakis. Hydrogen adsorption, absorption and diffusion on and in transition metal surfaces: A dft study. *Surface Science*, 606:679–689, 4 2012.
- [73] Aleksandar Staykov, Junichiro Yamabe, and Brian P. Somerday. Effect of hydrogen gas impurities on the hydrogen dissociation on iron surface. *International Journal of Quantum Chemistry*, 114:626–635, 5 2014.
- [74] Jun Song and W. A. Curtin. Atomic mechanism and prediction of hydrogen embrittlement in iron. *Nature Materials 2012 12:2*, 12:145–151, 11 2012.
- [75] Tao Lu, Guo Jian Niu, Yuping Xu, Jing Wang, Zhongqing An, Haodong Liu, Haishan Zhou, Fang Ding, Guang Nan Luo, and Xiao Chun Li. Molecular dynamics study of the diffusion properties of h in fe with point defects. *Fusion Engineering and Design*, 113:340–345, 12 2016.
- [76] A. Tehranchi and W. A. Curtin. Atomistic study of hydrogen embrittlement of grain boundaries in nickel: I. fracture. *Journal of the Mechanics and Physics of Solids*, 101:150–165, 2017.
- [77] Lili Gai, Yun Kyung Shin, Muralikrishna Raju, Adri C.T. Van Duin, and Sumathy Raman. Atomistic adsorption of oxygen and hydrogen on platinum catalysts by hybrid grand canonical monte carlo/reactive molecular dynamics. *Journal of Physical Chemistry C*, 120:9780–9793, 5 2016.
- [78] Mamadou Diarra, Hakim Amara, François Ducastelle, and Christophe Bichara. Carbon solubility in nickel nanoparticles: A grand canonical monte carlo study. *Physica Status Solidi (B) Basic Research*, 249:2629–2634, 2012.
- [79] Babak Sadigh, Paul Erhart, Alexander Stukowski, Alfredo Caro, Enrique Martinez, and Luis Zepeda-Ruiz. Scalable parallel monte carlo algorithm for atomistic simulations of precipitation in alloys. *Physical Review B - Condensed Matter and Materials Physics*, 85, 5 2012.
- [80] Vesselin I Yamakov. Parallel grand canonical monte carlo (paragrandmc) simulation code. Technical report, NASA, 2016.
- [81] Steve Plimpton. Fast parallel algorithms for short-range molecular dynamics. *Journal of Computational Physics*, 117:1–19, 3 1995.
- [82] James E Angelo, N R Moody, and M I Baskes. Trapping of hydrogen to lattice defects in nickel. *Modelling Simul. Mater. Sci. Eng.*, 3:289–307, 1995.
- [83] Daniel Faken and Hannes Jonsson. Systematic analysis of local atomic structure combined with 3d computer graphics. *Computational Materials Science*, 2:279–286, 1994.
- [84] Alexander Stukowski. Visualization and analysis of atomistic simulation data with ovito-the open visualization tool. *Modelling and Simulation in Materials Science and Engineering*, 18, 2010.

- [85] Michael Krone, John E Stone, Thomas Ertl, and Klaus Schulten. Fast visualization of gaussian density surfaces for molecular dynamics and particle system trajectories. *The Eurographics Association*, 2012.
- [86] Alexander Stukowski. Visualization and analysis of atomistic simulation data with ovito-the open visualization tool. *Modelling and Simulation in Materials Science and Engineering*, 18, 2010.
- [87] Peter Mahler Larsen, Søren Schmidt, and Jakob SchiØtz. Robust structural identification via polyhedral template matching. *Modelling and Simulation in Materials Science and Engineering*, 24, 5 2016.
- [88] Thomas Bonald, Bertrand Charpentier, Alexis Galland, and Alexandre Hollocou. Hierarchical graph clustering using node pair sampling. *arXiv*, 6 2018.
- [89] Pang-Nin. Tan, Michael. Steinbach, and Vipin. Kumar. *Introduction to data mining*. Pearson, 2018.
- [90] Manik Madhikermi, Sylvain Kubler, Jérémy Robert, Andrea Buda, and Kary Främling. Data quality assessment of maintenance reporting procedures. *Expert Systems with Applications*, 63:145–164, 11 2016.
- [91] J Kameda, T E Bloomer, A H Swanson, and D Y Lyu. Neutron irradiation and intergranular fracture in vanadium-20 wt *Journal of Nuclear Materials*, 252:1–12, 1998.
- [92] J Kameda, T E Bloomer, and D Y Lyu. Grain boundary segregation of impurities in neutron irradiated and thermally aged vanadium alloys. *Journal of nuclear materials*, 1998.
- [93] Jiming Chen, Shaoyu Qiu, Lin Yang, Zengyu Xu, Ying Deng, and Ying Xu. Effects of oxygen, hydrogen and neutron irradiation on the mechanical properties of several vanadium alloys. *Journal of nuclear materials*, 2002.
- [94] M. Herbig, D. Raabe, Y. J. Li, P. Choi, S. Zaefferer, and S. Goto. Atomic-scale quantification of grain boundary segregation in nanocrystalline material. *Physical Review Letters*, 112, 12 2013.
- [95] Ji Jung Kai, Fu Rong Chen, and Ting Shien Duh. Effects of grain boundary misorientation on radiation-induced solute segregation in proton irradiated 304 stainless steels. *Materials Transactions*, 2004.
- [96] Xuyang Zhou, Xiao Xiang Yu, Tyler Kaub, Richard L. Martens, and Gregory B. Thompson. Grain boundary specific segregation in nanocrystalline fe(cr). *Scientific Reports*, 6, 10 2016.
- [97] Pavel Lejček and Siegfried Hofmann. Thermodynamics and structural aspects of grain boundary segregation. *Critical Reviews in Solid State and Materials Sciences*, 20:1–85, 1995.

- [98] Prakash Parajuli, David Romeu, Viwanou Hounkpati, Rubén Mendoza-Cruz, Jun Chen, Miguel José Yacamán, Jacob Flowers, and Arturo Ponce. Misorientation dependence grain boundary complexions in  $\{111\}$  symmetric tilt al grain boundaries. *Acta Materialia*, 181:216–227, 12 2019.
- [99] Fei Gao, Xin Sun, and Mark Tschopp. The effects of the uncertainty of thermodynamic and kinetic properties on nucleation and evolution kinetics of cr-rich phase in fe-cr alloys. *Nuclear Energy Enabling Technology*, 09 2012.
- [100] Peter Schweizer, Amit Sharma, Laszlo Pethö, Emese Huszar, Lilian Maria Vogl, Johann Michler, and Xavier Maeder. Atomic scale volume and grain boundary diffusion elucidated by in situ stem. *Nature Communications*, 14, 12 2023.
- [101] Xuyang Zhou, Ali Ahmadian, Baptiste Gault, Colin Ophus, Christian H. Liebscher, Gerhard Dehm, and Dierk Raabe. Atomic motifs govern the decoration of grain boundaries by interstitial solutes. *Nature Communications*, 14, 12 2023.
- [102] M A Pouchon, L.-A Nordströ, and Ch Hellwig. *Comprehensive Nuclear Materials 3.25 Modeling of Sphere-Pac Fuel*. Elsevier, 2012.
- [103] Wei Zhang, Zengtong Jiao, Chi Zhang, linfeng He, Gang Xu, Xiaotong Chen, and Bing Liu. Diffusion of fission products in nuclear graphite: A review. *Nuclear Materials and Energy*, 29, 12 2021.
- [104] M. Suzuki P. Van Uffelen. *Comprehensive Nuclear Materials 3.19 Oxide Fuel Performance Modeling and Simulations*. Elsevier, 2012.
- [105] T. Nagashima, M. Koyama, A. Bashir, M. Rohwerder, C. C. Tasan, E. Akiyama, D. Raabe, and K. Tsuzaki. Interfacial hydrogen localization in austenite/martensite dual-phase steel visualized through optimized silver decoration and scanning kelvin probe force microscopy. *Materials and Corrosion*, 68:306–310, 3 2017.
- [106] T Schober and C Dieker. Observation of local hydrogen on nickel surfaces. *Metallurgical Transactions*, 1983.
- [107] Xiao Ye Zhou, Ji Hua Zhu, and Hong Hui Wu. Molecular dynamics studies of the grain-size dependent hydrogen diffusion coefficient of nanograined fe. *International Journal of Hydrogen Energy*, 46:5842–5851, 1 2021.
- [108] Yang He, Yunjuan Su, Haobo Yu, and Changfeng Chen. First-principles study of hydrogen trapping and diffusion at grain boundaries in gamma-fe. *International Journal of Hydrogen Energy*, 46:7589–7600, 2 2021.
- [109] Yi Luo, Wei Li, Laizhu Jiang, Ning Zhong, and Xuejun Jin. Hydrogen embrittlement and hydrogen diffusion behavior in interstitial nitrogen-alloyed austenitic steel. *International Journal of Hydrogen Energy*, 46:32710–32722, 9 2021.



- [110] Hiroshi Kakinuma, Saya Ajito, Tomohiko Hojo, Motomichi Koyama, and Eiji Akiyama. In situ visualization of misorientation-dependent hydrogen diffusion at grain boundaries of pure polycrystalline ni using a hydrogen video imaging system. *Acta Materialia*, 263, 1 2024.
- [111] Ruiwen Xie, Song Lu, Wei Li, Yanzhong Tian, and Levente Vitos. Dissociated dislocation-mediated carbon transport and diffusion in austenitic iron. *Acta Materialia*, 191:43–50, 6 2020.
- [112] Xiao Zhou, Normand Mousseau, and Jun Song. Is hydrogen diffusion along grain boundaries fast or slow? atomistic origin and mechanistic modeling. *Physical Review Letters*, 122, 5 2019.
- [113] Yi-Sheng Chen, Hongzhou Lu, Jiangtao Liang, Alexander Rosenthal, Hongwei Liu, Glenn Sneddon, Ingrid Mccarroll, Zhengzhi Zhao, Wei Li, Aimin Guo, and Julie M Cairney. Observation of hydrogen trapping at dislocations, grain boundaries, and precipitates. *Science*, 2020.
- [114] O. Barrera, D. Bombac, Y. Chen, T. D. Daff, E. Galindo-Nava, P. Gong, D. Haley, R. Horton, I. Katzarov, J. R. Kermode, C. Liverani, M. Stopher, and F. Sweeney. Understanding and mitigating hydrogen embrittlement of steels: a review of experimental, modelling and design progress from atomistic to continuum. *Journal of Materials Science*, 53:6251–6290, 5 2018.
- [115] Ziyang Zhou, Zhengquan Wang, Ranming Niu, Pang Yu Liu, Chao Huang, Yi Hsuan Sun, Xiutong Wang, Hung Wei Yen, Julie M. Cairney, and Yi Sheng Chen. Cryogenic atom probe tomography and its applications: a review. *Microstructures*, 3, 2023.
- [116] Baptiste Gault, Andrew J. Breen, Yanhong Chang, Junyang He, Eric A. Jäggle, Paraskevas Kontis, Philipp Kürnsteiner, Alisson Kwiatkowski Da Silva, Surendra Kumar Makineni, Isabelle Mouton, Zirong Peng, Dirk Ponge, Torsten Schwarz, Leigh T. Stephenson, Agnieszka Szczepaniak, Huan Zhao, and Dierk Raabe. Interfaces and defect composition at the near-atomic scale through atom probe tomography investigations. *Journal of Materials Research*, 33:4018–4030, 12 2018.
- [117] Andrew J. Breen, Leigh T. Stephenson, Binhuan Sun, Yujiao Li, Olga Kasian, Dierk Raabe, Michael Herbig, and Baptiste Gault. Solute hydrogen and deuterium observed at the near atomic scale in high-strength steel. *Acta Materialia*, 188:108–120, 4 2020.
- [118] Sheng Yin, Guangming Cheng, Tzu Hsuan Chang, Gunther Richter, Yong Zhu, and Huajian Gao. Hydrogen embrittlement in metallic nanowires. *Nature Communications*, 10, 12 2019.
- [119] G. M. Bond, I. M. Robertson, and H. K. Birnbaum. Effects of hydrogen on deformation and fracture processes in high-purity aluminium. *Acta Metallurgica*, 36:2193–2197, 1988.

- [120] G M Bond, I M Robertson, and H K Birnbaum. On the mechanisms of hydrogen embrittlement of ni,al alloys. *Acta metalii*, 37:1407–1413, 1989.
- [121] P J Ferreira, I M Robertson, and H K Birnbaum. Hydrogen effects on the character of dislocations in high-purity aluminum. *Acta Metallurgica*, 1999.
- [122] Degang Xie, Suzhi Li, Meng Li, Zhangjie Wang, Peter Gumbsch, Jun Sun, Evan Ma, Ju Li, and Zhiwei Shan. Hydrogenated vacancies lock dislocations in aluminium. *Nature Communications*, 7, 2016.
- [123] D S Sheit, I M Robertson, and H K Birnraum. Hydrogen embrittlement of a titanium: In sltu tem studies. *Acta metall*, 36:111–124, 1988.
- [124] I M Robertson and H K Birnbaum. An hvem study of hydrogen effects on the deformation and fracture of nickel. *Acra merall*, 34:353–366, 1986.
- [125] De Gang Xie, Liang Wan, and Zhi Wei Shan. Hydrogen enhanced cracking via dynamic formation of grain boundary inside aluminium crystal. *Corrosion Science*, 183, 5 2021.
- [126] G. Girardin, C. Huvier, D. Delafosse, and X. Feaugas. Correlation between dislocation organization and slip bands: Tem and afm investigations in hydrogen-containing nickel and nickel-chromium. *Acta Materialia*, 91:141–151, 6 2015.
- [127] G. Hachet, J. Li, A. M. Hallil, A. Metsue, A. Oudriss, J. Bouhattate, and X. Feaugas. A multi-scale analysis of the different interactions between defects and hydrogen: A review on the contribution of the elastic fields. *Engineering Fracture Mechanics*, 218, 9 2019.
- [128] Y. Yagodzinsky, T. Saukkonen, S. Kilpeläinen, F. Tuomisto, and H. Hänninen. Effect of hydrogen on plastic strain localization in single crystals of austenitic stainless steel. *Scripta Materialia*, 62:155–158, 2 2010.
- [129] Gouenou Girardin and David Delafosse. Solute-dislocation interactions: Modelling and experiments in hydrogenated nickel and nickel base alloys. *Materials Science and Engineering: A*, 387-389:51–54, 12 2004.
- [130] S. G. Srinivasan, M. I. Baskes, and G. J. Wagner. Atomistic simulations of shock induced microstructural evolution and spallation in single crystal nickel. *Journal of Applied Physics*, 101, 2007.
- [131] M F Horstemeyer, M I Baskes, A Godfrey, and D A Hughes. A large deformation atomistic study examining crystal orientation effects on the stress±strain relationship. *International Journal of Plasticity*, 2002.
- [132] S. G. Srinivasan, X. Z. Liao, M. I. Baskes, R. J. McCabe, Y. H. Zhao, and Y. T. Zhu. Compact and dissociated dislocations in aluminum: Implications for deformation. *Physical Review Letters*, 94, 4 2005.

- [133] Mei Q. Chandler, M. F. Horstemeyer, M. I. Baskes, G. J. Wagner, P. M. Gullett, and B. Jelinek. Hydrogen effects on nanovoid nucleation at nickel grain boundaries. *Acta Materialia*, 56:619–631, 2 2008.
- [134] James E Angelo and Michael I Baskes. Interfacial studies using the eam and meam. *INTERFACE SCIENCE*, 4:47–63, 1996.
- [135] Mei Q. Chandler, M. F. Horstemeyer, M. I. Baskes, P. M. Gullett, G. J. Wagner, and B. Jelinek. Hydrogen effects on nanovoid nucleation in face-centered cubic single-crystals. *Acta Materialia*, 56:95–104, 1 2008.
- [136] A. Drexler, S. He, R. Pippan, L. Romaner, V. I. Razumovskiy, and W. Ecker. Hydrogen segregation near a crack tip in nickel. *Scripta Materialia*, 194, 3 2021.
- [137] Yu Ding, Haiyang Yu, Meichao Lin, Michael Ortiz, Senbo Xiao, Jianying He, and Zhiliang Zhang. Hydrogen trapping and diffusion in polycrystalline nickel: The spectrum of grain boundary segregation. *Journal of Materials Science and Technology*, 173:225–236, 2 2024.